Development of Magnetic Nanostructured Silica-Based Materials as Potential Vectors for Drug-Delivery Applications

Manuel Arruebo,[†] Marta Galán,[†] Nuria Navascués,[†] Carlos Téllez,[†] Clara Marquina,[‡] M. Ricardo Ibarra,[†] and Jesús Santamaría*,[†]

Nanoscience Institute of Aragon (INA) and Materials Science Institute of Aragon (CSIC), University of Zaragoza, 50009 Zaragoza, Spain

Received July 26, 2005. Revised Manuscript Received October 31, 2005

Metallic iron nanoparticles were synthesized within micron-sized mesoporous molecular sieves (with 2.9-nm pores) and hollow silica microcapsules (pores of 2.7 and 15 nm) using several cycles of wet impregnation under vacuum, followed by drying, oxidation, and reduction steps. For iron-loaded MCM-48, SQUID measurements revealed ferromagnetic behavior at room temperature with a magnetic moment as high as 3.40 emu/g (measured at 2 T) after four deposition cycles. Iron-loaded hollow silica microcapsules (250-nm wall thickness) showed a magnetic moment of 2.40 emu/g (at 2 T) after three deposition cycles and a coercivity as low as 12.9 Oe.

Introduction

Conventional cancer treatments include surgery, radiation, and chemotherapy. Surgical removal and irradiation are mainly limited by accessibility to the tumor, whereas chemotherapy is restricted by the lack of selectivity toward tumor cells, often giving rise to severe side effects in healthy tissues. Drug-delivery systems with nano- and microparticles show a clear potential for cancer treatments in view of advantages such as (i) the ability to target specific locations in the body, (ii) the ability to reduce the quantity of drug that needs to be delivered to attain a particular concentration level in the vicinity of the target, and (iii) the ability to decrease the concentration of the drug at nontarget sites.[1] As a consequence, controlled drug delivery is one of the fastest-growing segments of the pharmaceutical market, and in the United States alone, the demand is expected to grow nearly 9% annually to reach more than $82 billion by 2007.[2]

The two primary challenges confronting drug-delivery systems are the achievement of a sustained delivery of the drug in the proximity of the diseased organ and the preferential targeting of malignant cells by the drug. These challenges can be addressed by acting on the characteristics of the particles and capsules that are proposed as delivery vectors.

Thus, for intravenously injected particles, biocompatibility of the drug carrier is the first requirement to reduce the uptake of nano- and microparticles by the macrophages of the reticulo-endothelial system (RES) and their consequent clearance to different organs depending on the different adsorption patterns of plasma proteins (opsonins).[3] The requirement of selective targeting to minimize damage to healthy tissue can be met by promoting specific carrier−target interactions (e.g., antigen−antibody interactions) or by means of the specific physicochemical properties of the carrier (e.g., magnetism, charge, hydrophobicity/hydrophilicity, specific affinity, pH).

Different organic materials such as polymeric nanoparticles, liposomes, and micelles have been investigated as drug-delivery vectors.[4] However, the search for different alternatives continues in view of a variety of still unsolved problems of these systems, such as their limited chemical and mechanic stability,[5] swelling, susceptibility to microbiological contamination, and inadequate control over the drug-release rate. On the other hand, many inorganic materials are nontoxic and biocompatible; present a high chemical and mechanical stability; and have a hydrophilic character and porous structure that can, in principle, be tailored to control the diffusion rate of an adsorbed or encapsulated drug. In this area, magnetic and nonmagnetic silica nanoparticles for drug-delivery systems can be prepared by means of the sol−gel procedure (e.g., ref 6), using silica xerogels, which are synthesized at room temperature,[7] laser pyrolysis,[8] and hydrothermal synthesis.

The so-called MCMs constitute a family of silica-based mesoporous structured materials that have been scarcely investigated as drug-delivery vectors, despite their interesting characteristics. Thus, MCMs exhibit large specific surface

* To whom correspondence should be addressed. E-mail: iqcatal@unizar.es.
[†] Nanoscience Institute of Aragon (INA).
[‡] Materials Science Institute of Aragon (CSIC-University of Zaragoza).

(1) Ritter, J.; Ebner, A.; Daniel, K.; Stewart, K. *J. Magn. Magn. Mater.* **2004**, *280*, 184.
(2) Sahoo, S. K.; Labhasetwart, V. *Drug Discov. Today* **2003**, *8*, 1112.
(3) Müller, R.; Lück, M.; Harnisch, S.; Thode, K. *Scientific and Clinical Applications of Magnetic Carriers*; Häfeli, U., Ed.; Plenum Press: New York, 1997; Chapter 10, p 141.
(4) Kumar, M. R. *J. Pharm. Pharm. Sci.* **2000**, *3*, 234.
(5) Barbé, C.; Bartlett, J.; Kong, L.; Finnie, K.; Qiang, H.; Larkin, M.; Calleja, S.; Bush, A.; Calleja G. *Adv. Mater.* **2004**, *16*, 1959.
(6) Veith, S. R.; Perren, M.; Pratsinis, S. E. *J. Colloid Interface Sci.* **2005**, *283*, 495.
(7) Kortesuo, P.; Ahola, M.; Kangas, M.; Yli-Urpo, A.; Kiesvaara, J.; Marvola, M. *Int. J. Pharmac.* **2001**, *221*, 107.
(8) Bomatí-Miguel, O.; Leconte, Y.; Morales, M. P.; Herlin-Boime, N.; Veintemillas-Verdaguer, S. *J. Magn. Magn. Mater.* **2005**, *272*−*275*, 290.

10.1021/cm051646z CCC: $33.50 © 2006 American Chemical Society
Published on Web 03/14/2006

areas and narrow pore-size distributions, with average pore diameters that can be selected between 15 and 100 Å by adjusting the synthesis conditions and/or by employing surfactants with different chain lengths in their preparation. Their regular pore openings can also be ordered in different arrays, including hexagonal (MCM-41), cubic (MCM-48), and lamellar (MCM-50). The main structural differences between MCMs and zeolites are that the later are microporous and crystalline structures, whereas the pore walls in the MCMs are formed by amorphous silica. Their specific ordering is given by the distribution of the mesopores, giving rise to the appearance of XRD peaks at $2\theta < 7°$.[9]

M41S mesoporous molecular sieves have been investigated as a possible aspirin-delivery vector by modifying their surface with aminopropyl groups that were then covalently linked to aspirin.[10] Ibuprofen,[11] bactericidal zinc(II) complexes,[12] and heparin[13] are also drugs that have been used to load silica-based materials. In addition, scientists from the National Institute of Advanced Industrial Science and Technology (AIST-Kansai), Osaka, Japan, have developed a modified MCM-41 material that opens or closes its pores under the influence of light,[14] offering the possibility of a photocontrolled release of guest molecules.

A volume-based rather than surface-based approach to drug delivery is also possible. Thus, unlike MCM particles, where the drug is loaded by adsorption on the surface area of the material, with hollow spheres or particles, the drug could also be stored in the empty inner volume, thus leading to higher loads per unit mass of vector. A variety of preparation methods is now available to produce silica-based hollow spheres, consisting of mesoporous silica or zeolites, and with or without functionalized interiors (e.g., Schult-Eklo et al.,[15] Caruso et al.,[16] Dong et al.,[17] Valtchev and Mintova[18]). These approaches could, in principle, be used in drug-delivery applications given their characteristics of biocompatibility and comparatively high drug loading capability. Thus, Zhu et al.[19] recently showed that hollow mesoporous silica spheres were able to hold a much higher amount of drug than conventional MCM-41 particles, with over one-half of the load stored in the hollow core.[19]

With both microparticles and microcapsules, magnetic behavior is desirable, to allow the use of magnetic fields to direct the delivery vectors and increase their residence time in the vicinity of the target area. However, it must be noted that most metals with strong magnetic behavior, such as iron or cobalt, show toxicity problems when they are present in quantities exceeding those required for accomplishing their biological functions,[20] and therefore, they need to be encapsulated in biocompatible covers to prevent redox reactions of those metals when they are free in the blood. Silica and related materials appear to be good candidates for this approach.

In this work, we have developed mesoporous silica particles belonging to the MCM family (MCM-41 and MCM-48), as well as hollow silica microcapsules. Iron was deposited inside the porous structures of both particles and microcapsules to obtain magnetic drug-delivery vectors. In both cases, the particle size enables transport through the vascular system, and the particles can be concentrated in the vicinity of the target with the aid of a magnetic field (which can be internal or external to the body). Once in position, the rate of drug release is controlled by the diffusion process out of the vector and into the body fluids. The release rate could, in principle, be controlled by adjusting the size and porous structure of the vector, so that the concentration of the drug at the desired location would remain within the optimum therapeutic range and under the toxicity threshold.

Experimental Section

Preparation of MCM-41 and MCM-48 Powders and Hollow Silica Microcapsules. MCM-41 particles were prepared according to the procedure given by Nishiyama et al.,[21] by means of a hydrothermal synthesis in a Teflon-lined autoclave, using an aluminosilicate solution in the presence of hexadecyltrimethylammonium bromide (CTABr) as the surfactant. A surfactant/Si molar ratio of 0.05 was used, and hydrothermal synthesis was carried out at 363 K for 96 h under autogenous pressure. MCM-48 particles were prepared according to the procedure of Fröba et al.,[22] also with CTABr as the surfactant. The synthesis gel molar composition used was $1TEOS/0.65CTABr/0.5KOH/62H_2O$. The hydrothermal synthesis conditions were 388 K for 48 h under autogenous pressure.

After synthesis, both powders were washed, filtered, and calcined in air at 823 K for 6 h with cooling and heating rates of 1 K/min.

Hollow silica microcapsules were prepared following the experimental procedure given by Schulz-Ekloff et al.,[15] with a slight variation in the composition of the synthesis gel. In our case, the molar composition was $1.5Na_2SiO_3/1CTABr/361H_2O/7.4CH_3COOC_2H_5$. The synthesis mixture was kept in a closed polypropylene container at room temperature for 5 h, and then synthesis proceeded at 363 K for 50 h in an open container. The obtained powder was washed in distilled water and ethanol and then filtered and calcined at 873 K for 6 h with cooling and heating rates of 1 K/min.

Encapsulation of Iron within the MCM Powders and the Hollow Silica Microcapsules. The wet impregnation technique was used to load iron within the structure of the prepared powder (particles) and microcapsules. In a typical procedure, the air contained within the pores and cavities of these materials was first removed under vacuum, and then, a 1.6 M $Fe(NO_3)_3 \cdot 9H_2O$ solution was admitted into the vessel to carry out impregnation at atmospheric pressure. After impregnation, the particles and microcapsules were dried at room temperature and under vacuum to avoid the premature formation of hematite outside the pores;[22] they were then

(9) Decyk, P.; Trejda, M.; Ziolek, M. *C. R. Chim.* **2005**, *8*, 635.
(10) Zeng, W., Qian, X. F.; Zhang, Y. B.; Yin, J.; Zhu, Z. K. *Mater. Res. Bull.* **2005**, *40*, 766.
(11) Vallet-Regi, M.; Rámila, A.; del Real, R. P.; Pérez-Pariente, J. *Chem. Mater.* **2001**, *13*, 308.
(12) Zeleňák, V.; Hornebecq, V.; Llewellyn, P. *Microporous Mesoporous Mater.* **2005**, *83*, 125.
(13) Ahola, M. S.; Säilynoja, E. S.; Raitavuo, M. H.; Vaahtio, M. M.; Salonen, J. I. *Biomaterials* **2001**, *22*, 2163.
(14) Mal, N. K.; Fujiwara, M.; Tanaka, Y. *Nature* **2003**, *421*, 350.
(15) Schult-Eklo, G.; Rathousk, J.; Zukal, A. *Int. J. Inorg. Mater.* **1999**, *1*, 97.
(16) Caruso, F.; Möhwald, H. *Science* **1998**, *282*, 1111.
(17) Dong, A.; Wang, Y.; Wang, D.; Yang, W.; Zhang, Y.; Ren, N.; Gao, Z.; Tang, Y. *Microporous Mesoporous Mater.* **2003**, *64*, 69.
(18) Valtchev, V.; Mintova, S. *Microporous Mesoporous Mater.* **2000**, *43*, 41.
(19) Zhu, Y.; Shi, J.; Chen, H.; Shen W.; Dong, X. *Microporous Mesoporous Mater.* **2005**, *84*, 218.
(20) Fraga C. G. *Mol. Aspects Med.* **2005**, *26*, 235.
(21) Nishiyama, N.; Park, D. H.; Koide, A.; Egashira, Y.; Ueyama, K. *J. Membr. Sci.* **2001**, *182*, 235.
(22) Fröba, M.; Köhn, R.; Bouffaud, G. *Chem. Mater.* **1999**, *1*, 2858.

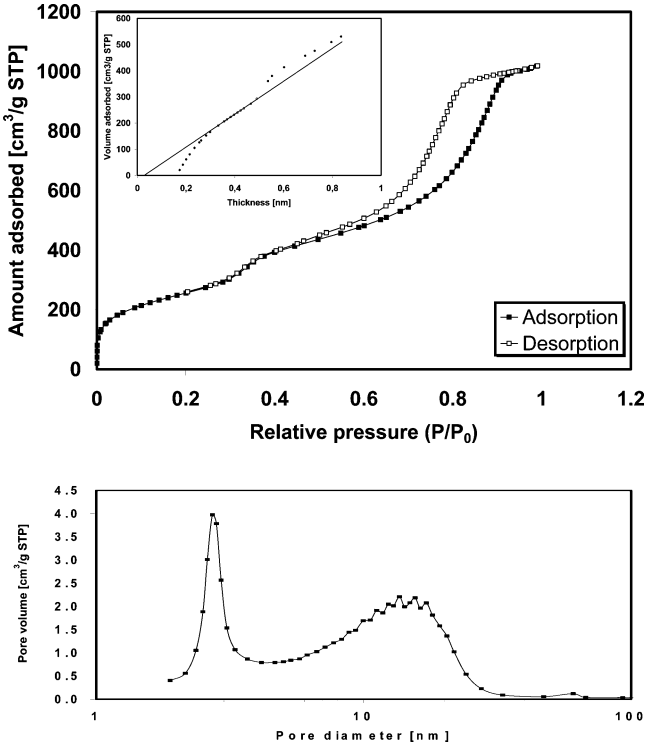

Figure 1. (a) N_2 adsorption/desorption isotherms and *t*-plot (inset) and (b) pore-size distribution plot calculated according to the BJH model of the desorption branch for hollow silica microcapsules.

heated under pure air to 673 K (heating rate of 1 K/min) and maintained at this temperature for 4 h. This oxidation process yielded α-Fe_2O_3, which was then reduced in H_2 at 800 K (heating rate of 3 K/min) to produce metallic iron. The impregnation/oxidation/reduction procedure could be repeated to increase the iron load on the particles and microcapsules.

Characterization. BET surface areas, N_2 adsorption/desorption isotherms, and pore-size distributions were obtained by means of a Micromeritics ASAP 2020 V1 device at 77 K.

Powder X-ray diffraction (XRD) was performed on a Rigaku/Max diffractometer using filtered Cu Kα radiation. The samples were also examined by scanning electron microscopy (SEM) in a JEOL JSM-6400 instrument operating at 3−20 kV, where energy-dispersive X-ray spectrometry (EDS) analysis was also carried out. Transmission electron microscopy (TEM) and selected-area electron diffraction (SAED) were also carried out on the samples. To obtain the high-resolution TEM (HRTEM) results, we used a JEOL 2010F field-emission gun microscope, which works at 200 kV and has a point-to-point resolution of 0.19 nm. Electron energy loss spectroscopy (EELS) spectra were obtained in a Gatan Image Filter (GIF 2000) coupled to the TEM microscope. The spectra obtained achieved an energy resolution of 1.2 eV.

Temperature-programmed reduction (TPR) experiments were carried out at atmospheric pressure in a quartz reactor loaded with 200 mg of a freshly calcined sample, under a mass-flow-controlled stream containing 6% H_2 in N_2. The sample was heated at 3 K/min, from room temperature to 800 K.

Finally, the magnetic properties of the compounds were measured at room temperature in a superconducting quantum interference device (SQUID MPMS-5S, Quantum Design) from 0 to 20000 Oe.

Results and Discussion

N_2 Adsorption Measurements. Figure 1 shows the N_2 adsorption/desorption type IV isotherm for the hollow silica microcapsules before being loaded with iron. From these results, a bimodal pore-size distribution with peaks at 2.7 and ~15 nm was obtained. The total pore volume of the sample was 1.63 cm^3/g, the micropore volume (calculated from the *t*-plot method) was nearly zero, and the BET surface area was 840.3 m^2/g.

Table 1. Pore Volume (cm^3/g) and Total Internal Volume[a] (cm^3/g) of the MCM-41 and MCM-48 Particles and Hollow Silica Microspheres

	MCM-41	MCM-48	silica microspheres
micropores	0	0	0
mesopores	0.81	0.79	1.63
internal cavity	0	0	0.62
total	0.81	0.79	2.28

[a] Corresponding to the maximum loading capacity.

Analysis of the corresponding N_2 adsorption/desorption results (not shown) for the initial MCM-41 and MCM-48 powders gave mean pore sizes of 3.7 and 3.5 nm, pore volumes of 0.81 and 0.79 cm^3/g, and surface areas of 734.2 and 762.4 m^2/g, respectively [pore-size distributions were calculated using the adsorption branch of the N_2 adsorption/desorption isotherm and the Barret−Joyner−Halenda (BJH) method]. In view of these results, the loading capacities of the three vectors investigated in this work (microcapsules, MCM-41, and MCM-48 particles) are summarized in Table 1. As can be seen, the highest potential loads can be achieved with the silica microspheres, largely on account of the volume corresponding to their internal cavity. After being loaded with iron within the mesoporous structure, the BET surface area for the iron-loaded MCM-48 particles was 406.8 m^2/g, a significant reduction compared to its initial value of 762.4 m^2/g. In the same way, the pore volume was reduced to 0.234 m^3/g, less than one-third of its initial value. Both data suggest that considerable amounts of iron were present inside the pore system of MCM-48.

X-ray Diffraction Analysis. Figure 2 shows the XRD patterns obtained for "as-prepared" MCM-48 and for iron-loaded MCM-48 after four cycles of impregnation/drying/oxidation and reduction [Fe^0, magnetite, and hematite patterns are also indicated; however, maghemite (γ-Fe_2O_3) patterns are not plotted because they are very similar to those of magnetite]. The characteristic (211) reflection appears for both as-prepared and iron-loaded MCM-48 at $2\theta = 2.75°$. The corresponding XRD patterns for MCM-41 powder (Figure 3) showed the typical (100) reflection for MCM-41 at 2.33° for the iron-loaded material. This indicates a displacement from the as-prepared sample, whose characteristic peak appears at 2.42° (larger *d* spacing). For both MCM-48 and MCM-41, it can be seen that a reflection characteristic of Fe^0 appears at ca. $2\theta = 44°$ only for the iron-loaded samples. Also, for both iron-containing samples, a reflection is hinted at $2\theta = 36°$, indicating the possible presence of some α-Fe_2O_3 (hematite) that has not been totally reduced.

MCMs show different XRD spacings depending on the length of the chain of the surfactant employed. The packing of the monodirectional channels following hexagonal symmetry forms the MCM-41. MCM-48 is formed by two systems of independent tree-directional channels following a cubic symmetry. Using CTABr as the surfactant, as we did in this work, the shift of XRD reflections to larger values

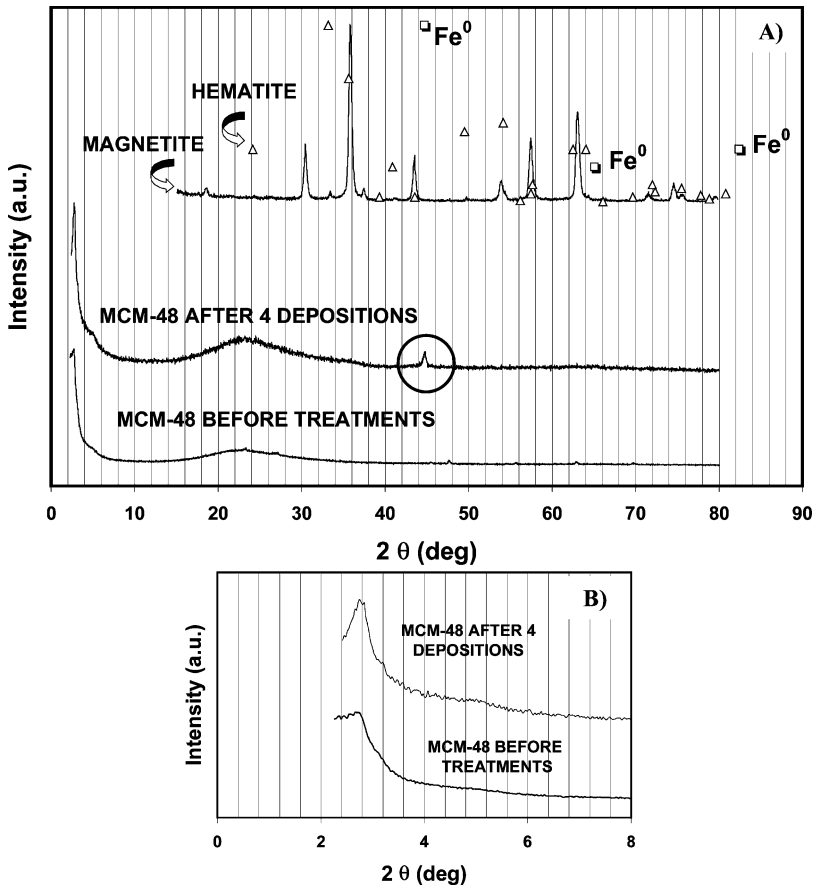

Figure 2. (A) X-ray diffraction patterns of magnetite, as-prepared MCM-48, and iron-loaded MCM-48 after four cycles of impregnation/drying/oxidation and reduction. For comparison, the reflections corresponding to hematite and Fe^0 are also shown. (B) Detailed view at low angles to show the characteristic peaks corresponding to mesoscopic ordering.

compared to the parent M41S can be attributed to the effect of the impregnation/calcination/reduction cycles, which might increase the degree of connectivity within the silica walls.[22]

Temperature-Programmed Reduction. The TPR profile of hollow silica microcapsules after three cycles involving deposition of iron precursors, oxidation, and reduction to form metallic iron is shown in Figure 4. The α-Fe_2O_3 formed within the silica structure showed a two-stage reduction, in agreement with previous reports in the literature.[23] In the first stage, hematite reduces to magnetite at ca. 475 K

$$3Fe_2O_3 + H_2 \rightarrow 2(FeO{\cdot}Fe_2O_3) + H_2O$$

The second peak at ca. 600 K corresponds to H_2 consumption for the reduction of magnetite to metallic iron

$$(FeO{\cdot}Fe_2O_3) + 4H_2 \rightarrow 3Fe + 4H_2O$$

The TPR diagram of Figure 4 seems to conform well to this description, although the ratio of the areas of the two peaks is 1:6.5, rather than 1:8 as it should be according to the stoichiometry of the two-stage reduction proposed. This would indicate that up to 20% of the magnetite might remain as such, rather than being reduced to metallic Fe. The difficulties in reducing iron in the channels of MCMs have already been pointed out by Köhn et al.,[24] who found that high temperatures were necessary to attain a fully reduced material.

Magnetic Measurements. The magnetic measurements carried out at room temperature for both the MCM particles and the silica microcapsules after iron loading are shown in Figure 5a. All of the curves present a hysteresis loop that is barely observable at the scale of Figure 5a, but can be appreciated in the close-up view of Figure 5b. It is important to point out that the magnetic moment values are given per unit of total mass (emu/g), that is, considering the total weight of both the silica and the iron in the particles or capsules. All of the samples showed ferromagnetic behavior. It can be seen (Figure 5a) that the magnetization loop does not reach the saturation magnetization, M_s in the interval of applied magnetic field (up to 2 T). As can be seen in the figure, the highest magnetization at 2 T was obtained for the iron-loaded MCM-48 sample, after four iron deposition cycles (3.40 emu/g). At the same applied field, the iron-loaded silica microspheres displayed a magnetization of 2.40 emu/g after three iron deposition cycles.

The remanence M_r, defined as the magnetization at $H = 0$, and the coercivity H_c, defined as the field magnitude necessary to obtain $M = 0$, can be read from Figure 5b, and the values are given in Table 2 for the different materials tested. After four depositions, iron-loaded MCM-48 showed a higher magnetic moment than MCM-41, in agreement with the higher intensity for the reflections corresponding to metallic iron

(23) Lin, Y.; Chen, Y. W.; Li, C. *Thermochim. Acta* **2003**, *400*, 61.

(24) Köhn, R.; Paneva, D.; Dimitrov, M.; Tsoncheva, T.; Mitov, I.; Minchev, C.; Fröba, M. *Microporous Mesoporous Mater.* **2003**, *63*, 125.

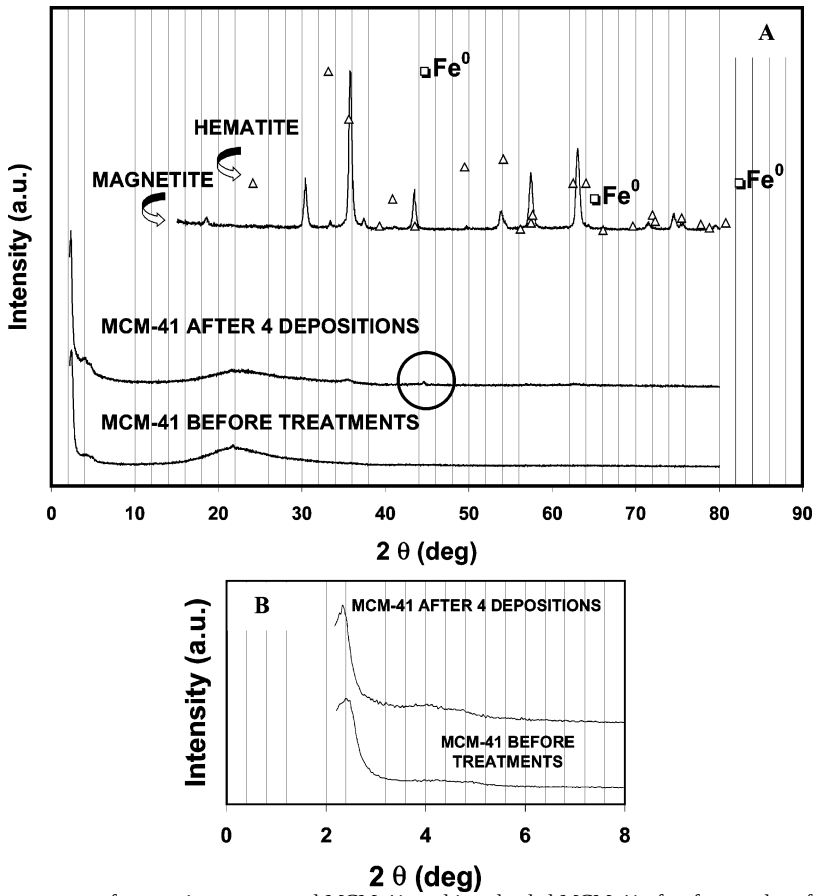

Figure 3. (A) X-ray diffraction patterns of magnetite, as-prepared MCM-41, and iron-loaded MCM-41 after four cycles of impregnation/drying/oxidation and reduction. For comparison, the reflections corresponding to hematite and Fe^0 are also shown. (B) Detailed view at low angles to show the characteristic peaks corresponding to mesoscopic ordering.

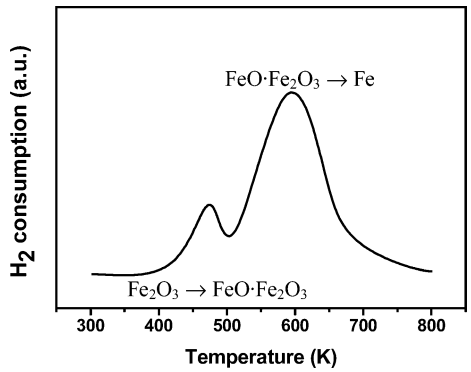

Figure 4. Temperature-programmed reduction profile obtained with a sample of hollow silica microcapsules after three iron-loading cycles.

Table 2. Magnetic Moment Measured at 2 T, Remanence, and Coercivity for the Mesoporous Molecular Sieves (M41S) and the Hollow Silica Microcapsules after Different Numbers of Iron Deposition Cycles

sample	no. of depositions	M^a (emu/g)	remanence M_r (emu/g)	coercivity H_c (Oe)
MCM-41	3	2.91	0.23	137.5
MCM-48	3	1.04	0.03	131.4
MCM-48	4	3.40	0.65	344.3
microspheres	3	2.40	0.01	12.9

[a] Measured at 2 T.

in the XRD patterns already discussed (Figures 1 and 2). Table 2 also shows that the coercivities were in the range of 130−350 Oe, except for the iron-loaded hollow silica microcapsules, which showed a coercivity as low as 12.9 Oe (together with the lowest remanence of all of the samples tested). These are desirable characteristics for drug-delivery applications: A sufficient magnetization under the presence of a magnetic field is desired to direct the vectors to the target region; however, once the magnetic field is eliminated, it is also required that the particles show a low tendency to form agglomerates, and this is aided by both a low remanence and a low coercivity.

Electron Microscopy. *MCM-41 and MCM-48 Particles.* Figures 6 and 7 show SEM photographs of iron-loaded MCM-41 and iron-loaded MCM-48 particles, respectively, after four cycles of deposition/oxidation/reduction. Most particles were shaped as regular spheres with a size between 1 and 4 μm. However, the presence of some loose material in the form of smaller-size aggregates between spheres could also be observed (Figure 7).

Examination using backscattered electrons during SEM observations did not reveal the presence of iron clusters on the surface of these particles at the resolution used in these measurements (Figures 6b and 7b). However, a more detailed examination using HRTEM did reveal iron clusters with a size of 20−100 nm that were present at (or very near) the surface of iron-loaded MCM-41 samples (Figure 8). For the iron-loaded MCM-48 particles, iron clusters with a size of 10−40 nm can also be seen on the external surface of the particles (Figure 9).

Electron energy loss (EELS) patterns (not shown) confirmed the presence of iron, as expected given the magnetic behavior displayed by these particles, together with Si and

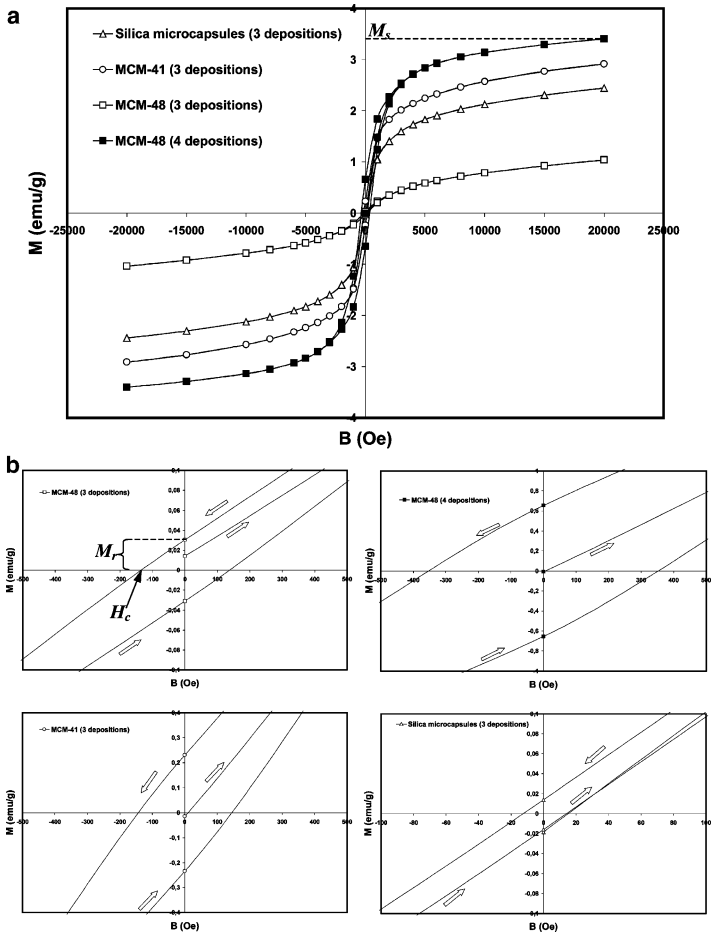

Figure 5. (a) Magnetic moment versus applied magnetic field at room temperature for the MCM samples and the hollow silica microcapsules after different numbers of iron deposition cycles. The magnetic moment (emu/g) is given per unit of total mass of the sample. (b) Detailed view of the region around the origin.

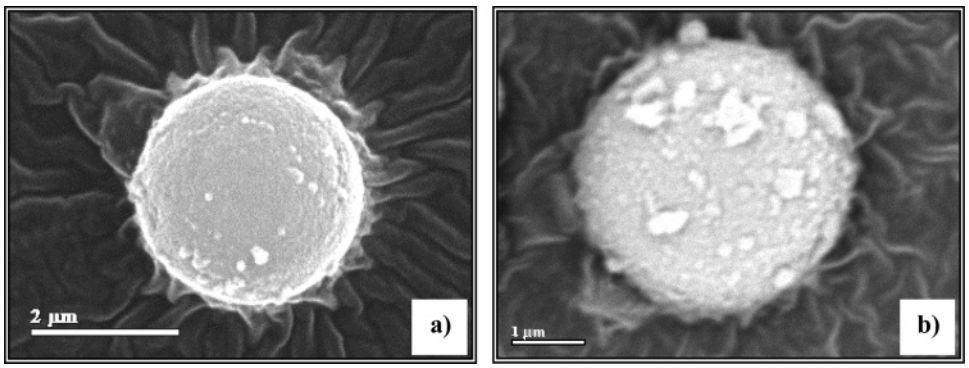

Figure 6. SEM images of MCM-41 particles after four iron deposition cycles. Right side: SEM image obtained using backscattered electrons.

O. No other elements were detected. Finally, the size of the channels measured by HRTEM was 2.95 ± 0.1 nm for iron-loaded MCM-41 and 2.9 ± 0.2 nm for iron-loaded MCM-48, in broad agreement with the mean pore sizes obtained from the N_2 adsorption measurements.

Silica Microcapsules. Figure 10 shows three SEM views of the iron-loaded hollow silica microcapsules after three iron deposition procedures. As can be seen, the spherical structure remains intact after several complete deposition cycles that, as seen above, involved heating in air to 673 K and reduction in H_2 at 800 K, with external diameters between 2 and 4 μm, the average diameter being around 3 μm. The wall thickness of the microcapsules is approximately 250−300 nm, as seen in the micrograph showing the broken capsule.

Iron clusters with a size of around 30 nm were observed near the surface of the iron-loaded silica microcapsules and were examined by selected-area electron diffraction (SAED). The SAED data showed the inverse spinel structure characteristic of magnetite (Figure 11), although the patterns could also be compatible with maghemite. The size of those clusters is larger than the dimensions found for the mesoporous channels of the hollow silica microspheres. Therefore, it is expected that iron oxide clusters of this size are located on either the external or internal surfaces of the hollow microspheres. However, smaller-size clusters (up to 15 nm) could be hosted inside the pore system of the iron-loaded silica spheres. The size of the channels measured by HRTEM was 2.0 ± 0.1 nm.

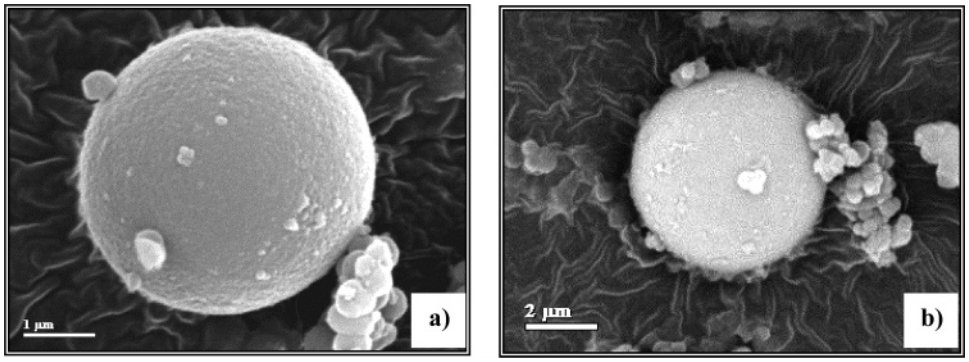

Figure 7. SEM images of MCM-48 particles after four iron deposition cycles. Right side: SEM image obtained using backscattered electrons.

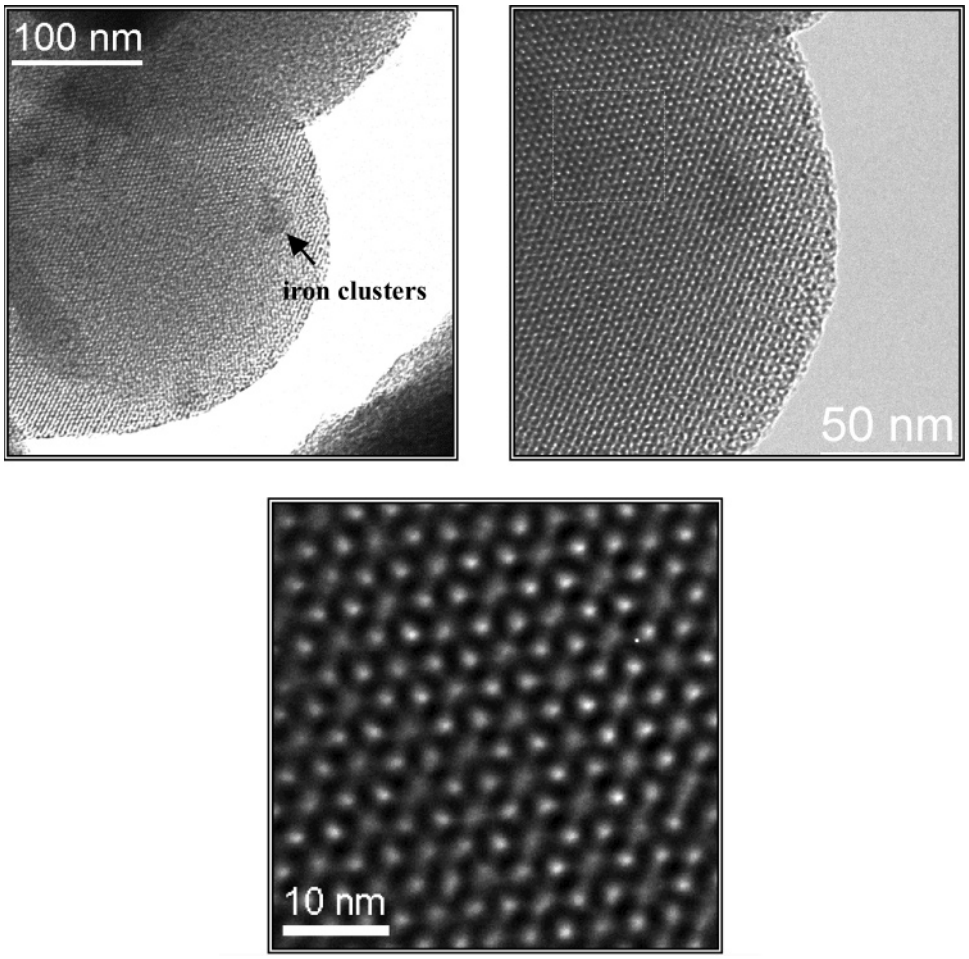

Figure 8. HRTEM images of iron-loaded MCM-41 particles.

Electron energy loss (EELS) patterns (not shown) again confirmed Fe, Si, and O as the only elements present in the iron-loaded silica microsphere sample, although, in this case, the spectra revealed three peaks in the range of 530−590 eV for oxygen (compared to only two peaks in the same region for the MCMs). This would be in agreement with the presence of mainly magnetite/maghemite particles on the observed region (outer surface) of hollow silica microspheres and metallic iron on the MCMs.

Discussion

Dong et al.[17] also used a wet impregnation technique to deposit iron on hollow zeolite microcapsules. Their procedure yielded randomly distributed clusters of α-Fe_2O_3 (hematite) with a size of around 13 nm. However, hematite is weakly magnetic, and this procedure did not yield magnetic particles (the authors' intention was only to show that different guest species such as Fe_2O_3 and Ag could be encapsulated inside the hollow silica microcapsules). In our work, after H_2 reduction, it is expected that mostly metallic iron is present on the different samples tested (both MCMs and microcapsules), given the fact that they were reduced in H_2 at 800 K and reduction to Fe^0 is already proceeding at 600 K, according to the TPR results (Figure 3).

However, it has also been shown that, because of their size, at least some of the iron clusters are located outside the pore system, on either the internal or external surface of the microspheres, where they are easily passivated (to magnetite or maghemite) with ambient oxygen, as shown

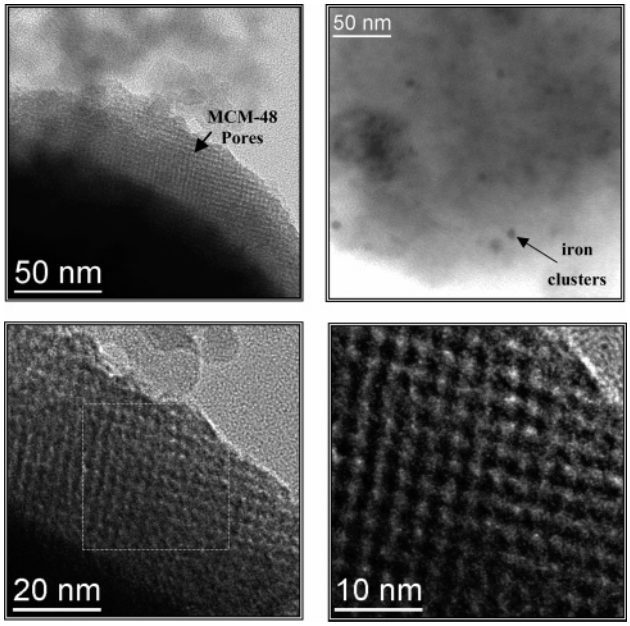

Figure 9. HRTEM images of iron-loaded MCM-48 particles

by the HRTEM results. It is also likely that elements within the porous structure of the iron-loaded MCM particles and the iron-loaded hollow silica microcapsules undergo reduction at a lower rate, and therefore, some clusters might remain as unreduced hematite. Nevertheless, most of the iron in the MCM particles seems to be present as a fully reduced species. This was clearly shown by the XRD results in the cases of MCM particles, where the bands observed at $2\theta = 44°$ constitute clear evidence that Fe^0 was present within the structures. The appearance of a weak reflection at $2\theta = 36°$ indicates that only a small amount of α-Fe_2O_3 (hematite) could remain unreduced in the iron-loaded MCM particles, in agreement with the TPR results discussed above.

The presence of mainly reduced iron is also consistent with the magnetic behavior shown by iron-loaded MCM particles. The magnetic susceptibility of the above-discussed iron phases increases in the order α-Fe_2O_3 (weakly magnetic) < $FeO{\cdot}Fe_2O_3$ < γ-Fe_2O_3 < Fe^0 (strongly magnetic). The degree of magnetization observed in Figure 5 (values as high as 3.40 emu/g were obtained at 2 T) therefore seems to confirm that most iron is reduced.

Regarding silica microspheres, the fate of iron clusters after the reduction process is probably mixed. It is well-known that iron oxidizes in oxygen atmosphere at room temperature to produce magnetite and maghemite (γ-Fe_2O_3) consecutively[25] or as a mixture of the two phases.[26] The thickness of this oxide film strongly depends on the exposure time, the temperature, and the oxidant agent used.[27] A further transition of maghemite to hematite generally requires temperatures above 573 K,[28] and therefore, it seems unlikely that any maghemite and magnetite phases produced by surface passivation during handing might be converted to hematite under low-temperature conditions. This is consistent with the SAED data, which showed the clusters on the outside of the silica microspheres to consist of magnetite. Nevertheless, it is reasonable to assume that iron clusters inside the mesopores of the iron-loaded microspheres will be more protected from oxidation and, therefore, that part of the metallic iron might remain as such inside the microspheres.

In summary, the above results show that, by the above-described iron deposition cycles, it is possible to obtain silica-based particles with a high magnetic moment compared to similar materials. Thus, by way of comparison, in a recent work, Liu et al.[29] used wet impregnation of iron acetylacetonate to obtain MCM-41 particles loaded with iron. The saturation magnetization and coercivity were 1.94 emu/g and 75 Oe, respectively. In this work, three to four iron deposition

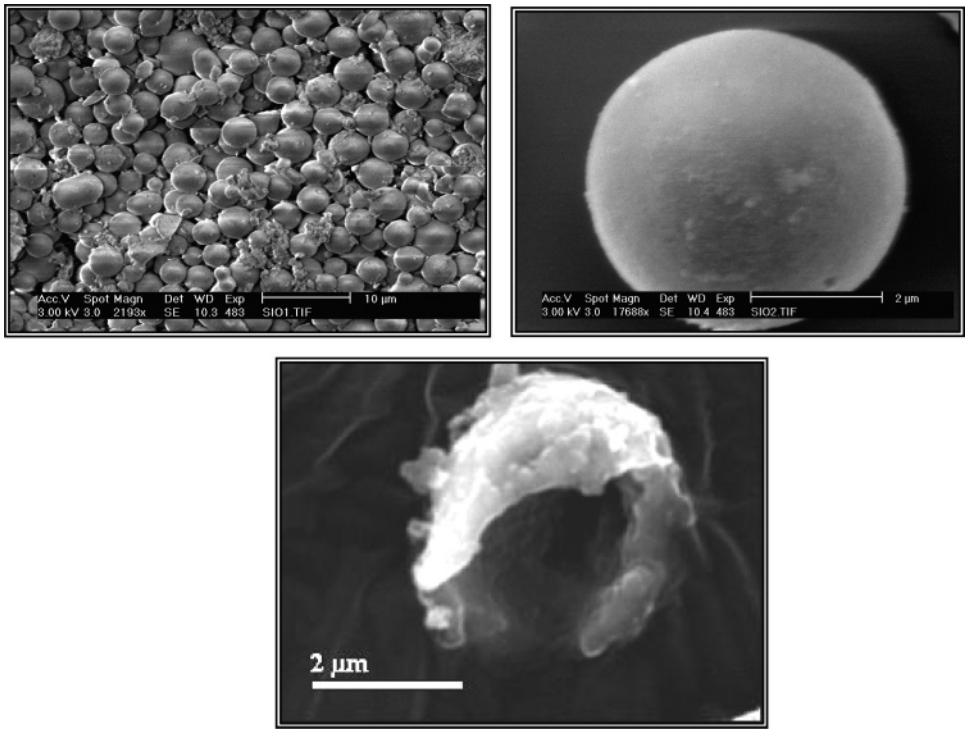

Figure 10. SEM images of hollow silica microcapsules after three iron deposition cycles. A broken capsule is also shown (bottom).

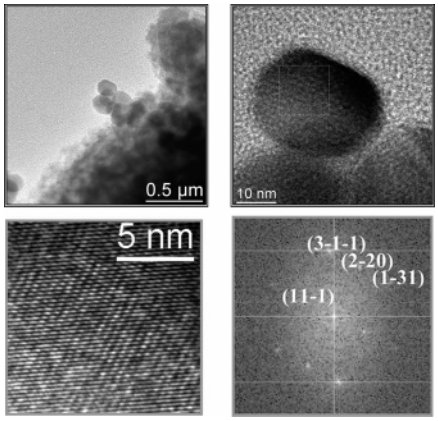

Figure 11. (Top) HRTEM images of the hollow silica microcapsules after three iron deposition cycles. (Bottom) Selected-area electron diffraction (SAED) patterns of the external magnetite/maghemite particles on the surface of the hollow silica microcapsules.

cycles are sufficient to obtain a higher magnetic moment for any of the materials tested. It must be noted, however, that only the iron-loaded microspheres showed a lower coercivity than the material of Liu et al.[29]

Finally, two main issues need to be addressed concerning the possible use of the silica-based magnetic particles developed in this work as drug-delivery vectors. First, particle size is important because the ability of the particles to reach a given location in the body is limited by the size of the vessels of the human circulatory system, with radii of 0.08−7.5, 0.005−0.07, and 0.004 mm for arteries, arterioles, and capillaries, respectively.[1] Almost all of the particles and microcapsules prepared in this work are below the limiting size for human capillaries (4-μm radius). In any case, the size of the particles can be decreased by adjusting the synthesis conditions and/or by employing surfactants with different chain lengths in their preparation. Alternatively, postsynthetic separation is easily done with physical methods such as filtration, sedimentation, or mild centrifugation.

The second issue concerns the presence of iron. The fact that SEM images obtained using backscattered electrons (Figures 6b and 7b) did not show large iron clusters on the surface of the iron-loaded particles indicates that iron is mainly located within the channels, which is in agreement with the work of Fröba et al.[22] However, using HRTEM, some iron clusters were observed on or close to the external surface of both iron-loaded MCM-41, and iron-loaded MCM-48 particles. The presence of exposed iron clusters must be minimized, as iron can sometimes have undesired health effects.[30] For the iron-loaded hollow silica microcapsules, this seems to be less of a problem, as iron on the surface readily converts into magnetite, a material of higher biocompatibility at the doses used in drug-delivery systems (e.g., ref 31).

Conclusions

Successive cycles of wet impregnation using iron nitrate under vacuum followed by drying, calcination, and reduction processes yielded metallic iron inside and on the external surface of MCM mesoporous silica particles and hollow silica microspheres. The incorporation of iron preserves the specific ordering of both iron-loaded MCM-41 and iron-loaded MCM-48 given by the distribution of their mesopores. For iron-loaded MCM-48, after four iron deposition cycles, it was possible to obtain a magnetic moment as high as 3.40 emu/g at 2 T. On the other hand, the iron-loaded microcapsules showed a magnetic moment of 2.40 emu/g after three deposition cycles, together with a coercivity of only 12.9 Oe. Furthermore, because of the high volume of their internal cavities, the microspheres are capable of delivering a higher drug load. Both groups of materials can therefore be considered as very promising materials for application in drug delivery.

Acknowledgment. We thank Mr. Rodrigo Fernández-Pacheco for valuable help with the SQUID measurements and Ms. Laura Casado for recording the SEM images. M.A. acknowledges the support of a contract from the "Juan de la Cierva" program (Project PPQ2003-04986). Support from the Spanish Nanoscience Action NAN200409270-C3-1/2 is gratefully acknowledged.

CM051646Z

(25) Lin, T. C.; Seshadri, G.; Kelber, J. A. *Appl. Surf. Sci.* **1997**, *119*, 83.
(26) Grosvenor, A. P.; Kobe, B. A.; McIntyre, N. S. *Surf. Sci.* **2004**, *565*, 151.
(27) Grosvenor, A. P., Kobe, B. A.; McIntyre, N. S. *Surf. Sci.* **2005**, *574*, 317.
(28) Cornell, R. M.; Schwertmann, U. *The Iron Oxides*; VCH: Weinheim, Germany, 1996.
(29) Liu, S.; Wang, Q.; van der Voort, P.; Cool, P.; Vansant, E. F.; Jiang, M. *J. Magn. Magn. Mater*. **2004**, *280*, 31.
(30) Walczyk, T.; von Blanckenburg, F. *Int. J. Mass Spectrosc.* **2005**, *242*, 117.
(31) Saravanan, M.; Bhaskar, K.; Maharajan, G.; Pillai, K. S. *Int. J. Pharm.* **2004**, *283*, 71.